

# Top quark flavor changing couplings at a muon collider.

Daniel Aké<sup>\*</sup>, Antonio O. Bouzas<sup>†</sup> and F. Larios<sup>‡</sup>  
 Departamento de Física Aplicada, CINVESTAV-Mérida,  
 A.P. 73, 97310 Mérida, Yucatán, México

November 22, 2024

## Abstract

There is growing interest in the development of a muon collider that would make it possible to produce lepton collisions at energies of several TeV. Among others, there can be significant contributions to electroweak gauge boson, Higgs boson and top quark physics. In this work we pay attention to the latter, in particular, effective flavor-changing (FC) top-quark interactions. We discuss the flavor changing  $t\bar{q}$  ( $q = u, c$ ) production processes that can be a good probe of the dimension-six top quark four-fermion and fermion-boson operators in the SMEFT. We consider all sixteen operators that can generate flavor-changing top quark couplings. After comparing with the current LHC bounds, we find potential limits three or four orders of magnitude stronger for four-fermion operators. Concerning fermion-boson couplings, for the tensor operators  $Q_{uW}$  and  $Q_{uB}$  we obtain the highest sensitivity. We also observe that the effective  $W$  approximation (EWA) does not apply with  $Q_{uB}$ .

## 1 Introduction

Due to the unique combination of accessible high energy collisions and a relatively clean environment, there has been renewed interest in the future construction of a muon collider (MuC) [1–3]. One outstanding purpose of the MuC is that, in principle, it could produce the Higgs boson at the resonance energy [4]. However, in recent years there is more interest in studying the potential of a MuC at high energies to probe the Higgs boson couplings [5–10]. In addition, there are also studies on the top quark [11, 12], the bottom quark [13–15],  $W$  boson scattering [16], and other processes [17–21].

In this work, we discuss the potential sensitivities that the MuC can reach at different energies for flavor changing (FC) dimension six operators. Besides the  $\mu\mu tu$  contact terms, we consider operators that generate effective couplings of the top quark and the gauge bosons [22]. Our purpose is to make a preliminary, but comprehensive assessment of all the possible FC top quark couplings. We find out which operators have little sensitivity and which ones have the highest sensitivity. Then, in future more in-depth studies we can focus on the latter. We also make a comparison with the current limits obtained by the LHC measurements on FC top-quark decays.

Concerning the current status of the MuC project, there is one energy, of 10 TeV that is considerably high and at the same time is seen upon as realistic in terms of cost and technical feasibility [1]. It should be able to achieve about  $10 \text{ ab}^{-1}$  of integrated luminosity and would probably be built after initial stages at lower energies are constructed. In this study, we are interested in this energy in particular, but we also include other energies and their respective luminosities, as they are presented in the recent literature. In table 1 we show the four energies and their potential integrated luminosities that we use. They have

---

<sup>\*</sup>daniel.ake@cinvestav.mx

<sup>†</sup>abouzas@cinvestav.mx

<sup>‡</sup>francisco.larios@cinvestav.mx, corresponding author.

been specifically proposed in ref. [3]. As seen from the table, the integrated luminosity grows with the collision energy, and we expect this feature to bring about stronger limits from top quark production.

$(\sqrt{s})(\text{TeV})$	3	6	10	14
$\mathcal{L}(\text{ab}^{-1})$	1	4	10	20

Table 1: Benchmark values for energy and luminosity of a high energy MuC [3].

The outline of the article is as follows. In section 2 we identify all the possible dimension-six operators relevant for top-quark production at the MuC. In section 3 we discuss the two most important modes of production, at tree level and with the top quark as final state:  $\mu^+ \mu^- \rightarrow t\bar{u}$  and  $\mu^+ \mu^- \rightarrow t\bar{u}\nu_\mu\bar{\nu}_\mu$ . At this level of approximation we make a simple estimate of the different sensitivities, and identify the two operators with the highest potential. In section 4 we make a more detailed analysis of the second mode of production, focused on the operators  $Q_{uB}^{k3}$ ,  $Q_{uB}^{3k}$ ,  $Q_{uW}^{k3}$ ,  $Q_{uW}^{3k}$ , with  $k = 1, 2$ . We consider the top hadronic decay channel and perform a signal and background analysis to obtain limits on the corresponding Wilson coefficients  $C_{k3,3k}^{uB}$  and  $C_{k3,3k}^{uW}$ . In section 5 we present our conclusions. Finally, in appendix A we make some brief comments on the definition of the dimension-six operator coefficients when going from gauge- to mass-eigenstate fields. In addition, recent limits on fermion-boson operators from the ATLAS collaboration are given in appendix B.

## 2 Operators with FC top quark couplings.

We refer to the list of dimension-six effective operators that is widely known as the Warsaw basis that first appeared in ref. [23]. This list was introduced in the basis of gauge eigenstates (tables 2 and 3). We want to work in the mass eigenstate basis, so we actually refer to ref. [24] which is a follow-up of [23]. In [24] the redefinition from the gauge to the mass eigenstate basis is thoroughly discussed and Feynman rules in  $R_\xi$ -gauges are provided. In table 2 there are nine fermion-boson operators that involve up-type quarks, and in table 3 there are seven four-fermion operators with up-type quarks and leptons. The operators in table 2 that generate top quark FC couplings with gauge bosons are [24]:

$$\begin{aligned}
Q_{u\varphi}^{(pr)} &= (\varphi^\dagger \varphi)(\bar{q}_p u'_r \tilde{\varphi}) \rightarrow [Htu] , \\
Q_{\varphi u}^{(pr)} &= (\varphi^\dagger i \overset{\leftrightarrow}{D}_\mu \varphi)(\bar{u}'_p \gamma^\mu u'_r) \rightarrow [Ztu] , \\
Q_{\varphi ud}^{(pr)} &= i(\tilde{\varphi}^\dagger \overset{\leftrightarrow}{D}_\mu \varphi)(\bar{u}'_p \gamma^\mu d'_r) \rightarrow [Wtd, Wub] , \\
Q_{\varphi q}^{(1)(pr)} &= (\varphi^\dagger i \overset{\leftrightarrow}{D}_\mu \varphi)(\bar{q}'_p \gamma^\mu q'_r) \rightarrow [Ztu, Zub] , \\
Q_{\varphi q}^{(3)(pr)} &= (\varphi^\dagger i \overset{\leftrightarrow}{D}_\mu^k \varphi)(\bar{q}'_p \tau^k \gamma^\mu q'_r) \rightarrow [Ztu, Zub, Wtd, Wub] , \\
Q_{uG}^{(pr)} &= (\bar{q}'_p \sigma^{\mu\nu} T^a u'_r) \tilde{\varphi} G_{\mu\nu}^a \rightarrow [Gtu] , \\
Q_{uB}^{(pr)} &= (\bar{q}'_p \sigma^{\mu\nu} u'_r) \tilde{\varphi} B_{\mu\nu} \rightarrow [\gamma tu, Ztu] , \\
Q_{uW}^{(pr)} &= (\bar{q}'_p \sigma^{\mu\nu} u'_r) \tau^k \tilde{\varphi} W_{\mu\nu}^k \rightarrow [\gamma tu, Ztu, Wtd, Wub] , \\
Q_{dW}^{(pr)} &= (\bar{q}'_p \sigma^{\mu\nu} d'_r) \tau^k \varphi W_{\mu\nu}^k \rightarrow [\gamma ub, Zub, Wtd, Wub] ,
\end{aligned} \tag{1}$$

where, for clarity, we have indicated the effective vertices generated by each operator in square brackets. We are interested in the case where one of the flavor indices  $pr$  is equal to 3 and the other one is 1 or 2. Due to the high energy of the processes of interest the charm quark can be taken as massless and there is no difference between  $t\bar{u}$  and  $t\bar{c}$  production. Therefore, we will usually refer to specific flavor indices 13 and 31, with the understanding that our results are equally valid for 23 and 32.

The operators in table 3 that generate contact terms of up quarks and leptons are [24]:

$$\begin{aligned}
Q_{lq}^{(1)} &= (\bar{\ell}_p' \gamma_\nu \ell_r') (\bar{q}_s' \gamma^\nu q_t') , \\
Q_{lq}^{(3)} &= (\bar{\ell}_p' \gamma_\nu \tau^k \ell_r') (\bar{q}_s' \gamma^\nu \tau^k q_t') , \\
Q_{eu} &= (\bar{e}_p' \gamma_\nu e_r') (\bar{u}_s' \gamma^\nu u_t') , \\
Q_{lu} &= (\bar{\ell}_p' \gamma_\nu \ell_r') (\bar{u}_s' \gamma^\nu u_t') , \\
Q_{qe} &= (\bar{e}_p' \gamma_\nu e_r') (\bar{q}_s' \gamma^\nu q_t') , \\
Q_{lequ}^{(1)} &= (\bar{\ell}_p' j e_r') \epsilon_{jk} (\bar{q}_s' k u_t') , \\
Q_{lequ}^{(3)} &= (\bar{\ell}_p' j \sigma^{\alpha\beta} e_r') \epsilon_{jk} (\bar{q}_s' k \sigma_{\alpha\beta} u_t') .
\end{aligned} \tag{2}$$

Where, in operator  $Q_{qe}$  we have changed the order of the quark and lepton terms so as to keep the same arrangement of all the other operators. As in the case of fermion-boson operators, we will be interested in the flavor indices  $prst = 2213$  that are related to  $\mu^+ \mu^- \rightarrow \bar{u}t$ . The numerical results for  $\bar{t}u$ ,  $\bar{c}t$  and  $\bar{t}c$  production are the same.

Looking at equation (1), let us observe that two operators generate FCNC couplings with up type quarks as well as with down type quarks:  $Q_{\varphi q(1)}$  and  $Q_{\varphi q(3)}$ . As far as FC charged currents are concerned, operators  $Q_{\varphi ud}$ ,  $Q_{\varphi q(3)}$ ,  $Q_{uW}$  and  $Q_{dW}$  also generate couplings with or without the top quark, depending on what combination of indices is considered: either 13 or 31. In one case the operator coefficient can only be probed via top quark production or top decay, and in the other case we could have bottom quark production or B meson decay as another good probe for the coefficient. In particular, concerning operators  $Q_{\varphi q}^{(1)}$  and  $Q_{\varphi q}^{(3)}$ , the following combinations are usually defined in the literature [25]:

$$\begin{aligned}
Q_{\varphi q(-)} &\equiv Q_{\varphi q}^{(1)} - Q_{\varphi q}^{(3)} , \\
Q_{\varphi q(+)} &\equiv Q_{\varphi q}^{(1)} + Q_{\varphi q}^{(3)} .
\end{aligned} \tag{3}$$

Where the  $Q_{\varphi q(-)}$  operator generates  $Ztu$  and  $Wtd$ ,  $Wub$  couplings, whereas  $Q_{\varphi q(+)}$  generates  $Zbd$  and  $Wtd$ ,  $Wub$ . In previous studies, it is assumed that  $Q_{\varphi q(+)}$  will be strongly bound by some down-quark FCNC process and therefore not included in a discussion of top quark production or decay [25]. While this is clearly justified, we point out two things: 1) in a future global analysis it may still be important to consider the contribution from  $Q_{\varphi q(+)}$  if the sensitivity is good enough for top production, and 2) as a matter of fact, the other operator  $Q_{\varphi q(-)}$  also generates a  $Wub$  coupling, which contributes to B meson decay at tree level so it also gets strong bounds [14]. Concerning four-fermion operators, we will use a similar combination [25]:

$$Q_{lq-} = \frac{1}{2}(Q_{lq}^{(1)} - Q_{lq}^{(3)}) ,$$

that separates the vertices  $\mu uut$  and  $\mu udb$ .

The Lagrangian in terms of interaction eigenstates is written as (omitting flavor indices):

$$\begin{aligned}
\mathcal{L} &= \mathcal{L}_{\text{SM}} + \frac{1}{\Lambda^2} C'_X Q_X \text{Hermitian} \\
&+ \frac{1}{\Lambda^2} (C'_Y Q_Y + C'^\dagger_Y Q_Y^\dagger) ,
\end{aligned} \tag{4}$$

where we will set the mass scale  $\Lambda = 1$  TeV for convenience. It is worthwhile to bear in mind that in this effective Lagrangian framework, the amplitudes we compute are valid as long as the process takes place at energies (well) below the scale  $\Lambda$ . For instance, at  $\sqrt{s} = 3$  TeV  $\Lambda$  should be about 10 TeV or higher. Of course, we do not know the scale of new physics and in presenting limits it would be appropriate to

refer to  $C_Q/\Lambda^2$  instead of just the coefficient  $C_Q$ . However, it is also customary to set  $\Lambda = 1\text{TeV}$  and the reader can infer that the number presented as a limit would be given in units of  $\text{TeV}^{-2}$  for  $C_Q/\Lambda^2$  (see ref. [25] for example). The Lagrangian of eq. (4) is the basis of what is known as the Standard Model Effective Field Theory (SMEFT). For a recent general and in-depth discussion of this topic we would like to refer to the article [26] by G. Isidori, F. Wilsch and D. Wyler, where issues about the validity of this framework are reviewed. For instance, if we were to compute the contribution of one of these top quark operators to the amplitude of the  $b \rightarrow s\gamma$  decay, we would refer to a matching scale  $\Lambda = M_W$  equal to the  $W$  boson mass (see fig. 10 in [26]). The effective operator of the Light Effective Field Theory (LEFT) that is used to compute the decay width receives contributions from operators of the SMEFT at the matching scale. Then, a renormalization group running is performed to obtain the value of this operator at the  $m_b$  scale, which is the relevant scale for this process. Similarly, there is a Beyond Standard Model theory that supersedes the SMEFT at a certain matching scale  $\Lambda_{\text{BSM}}$ . Of course, we do not know what is  $\Lambda_{\text{BSM}}$ . When a phenomenological study is done we have to refer to a certain energy scale that is appropriate for the study, one that is supposed to be below  $\Lambda_{\text{BSM}}$ . The limits that we will obtain for these operators are assumed to be taken at the energy scale of the production process, which for the MuC we have chosen to be one of the four values in particular: 3, 6, 10 and 14 TeV. In each case we are assuming that  $\Lambda_{\text{BSM}}$  is above that energy in particular. Strictly speaking, when we compare our limits with the current limits from LHC measurements we should be aware that there will be a renormalization group running from the scale of the collision energy down to the appropriate energy scale of the LHC. This may result in a variation of the order of 10%. We are not interested in making such detailed analysis in this study.

Operators  $Q_{\varphi u}$ ,  $Q_{\varphi q(-)}$  and  $Q_{\varphi q(+)}$  are Hermitian. The next step in our analysis is to re-write the operators and their Wilson coefficients in the mass eigenstate basis. For this we refer to ref. [24] where all the dimension-six operators are considered and the transition from interaction to mass eigenstates is discussed. We follow the treatment in [24], with some minor variations discussed below in appendix A. It is useful to establish the number of free parameters in our list of 9 fermion-boson operators. Let us consider the flavor index  $a = 1$ . We have three Hermitian operators and their coefficients must satisfy the condition  $C_{13} = C_{31}^*$ . Otherwise,  $C_{13}$  and  $C_{31}$  are independent. We thus have  $3 + 12 = 15$  complex free parameters for  $a = 1$ . For simplicity, however, in this study we consider them to be real numbers. Therefore, we are not considering CP violation effects in this study. In principle, all operators can give a contribution to some single top production process at the MuC. In trying to be comprehensive, we have checked the potential for each and every coefficient. It turns out that, only nine independent real couplings (3 + 6) will actually be relevant to our analysis. The reason is that for three operators,  $Q^{\varphi ud}$ ,  $Q^{uG}$  and  $Q^{dW}$  the contribution to any  $t\bar{t}$  production process will be either zero (by taking  $m_d = 0$ ) or negligible. So that their potential MuC limits will be two or more orders of magnitude weaker than current limits, and they will not appear in any of the tables where we show our results.

Let us now refer to four-fermion operators. They give rise to the two-to-two process  $\mu^+\mu^- \rightarrow t\bar{t}$  (or  $u\bar{t}$ ). (The lepton flavor indices are always  $pr = 22$  and there is no need to include them.) There are seven operators in equation (2) with the first five being Hermitian. So we have 4 + 4 independent coefficients:  $C_{1+3}^{lq-}$ ,  $C_{1+3}^{eu}$ ,  $C_{1+3}^{lu}$ ,  $C_{1+3}^{qe}$ ,  $C_{13}^{lequ1}$ ,  $C_{31}^{lequ1}$ ,  $C_{13}^{lequ3}$  and  $C_{31}^{lequ3}$  [25].

Given the energies of order TeV consider here, we have that terms of order  $m_t/\sqrt{s}$  are small. It is reasonable to assume massless fermions in the calculation of the cross section. In this case the contact terms give rise to very simple helicity amplitudes and associated production cross sections. By using the expressions provided in a previous work [27] we obtain:

$$\begin{aligned} \frac{\sigma_{\mu^+\mu^-\rightarrow t\bar{t}}}{\sigma_{1234}} &= |C_{1+3}^{lq-}|^2 + |C_{1+3}^{eu}|^2 + |C_{1+3}^{lu}|^2 + |C_{1+3}^{qe}|^2 \\ &+ \frac{3}{4}(|C_{13}^{lequ1}|^2 + |C_{31}^{lequ1}|^2) + 4(|C_{13}^{lequ3}|^2 + |C_{31}^{lequ3}|^2). \end{aligned} \quad (5)$$

Where  $\sigma_{1234} = s/(16\pi\Lambda^4)$  is the total cross section coming from the helicity structure  $[[12][34]]^2 = s^2$  discussed in Ref. [27]. Numerically, for  $\Lambda = 1\text{TeV}$  and  $\sqrt{s} = 3\text{TeV}$ , we get a rather high  $\sigma_{1234} \simeq 70\text{pb}$ . We have computed  $\sigma_{1234}$  with  $m_t$  not zero and the numerical difference is less than 3%. We will show limits for the four-fermion coefficients in the next section.

### 3 Single top production at the MuC.

In the SM, production of single top at a lepton collider comes from the process  $\ell^+\ell^- \rightarrow t\bar{b}W^- + \bar{t}bW^+$  and it can be used to probe the diagonal terms of the Wilson coefficients [28]. Single-top production that involves FC couplings can be given by  $\mu^+\mu^- \rightarrow t\bar{u} + u\bar{t}$  as shown in fig. 1. This top production mode is possible even with a low collision energy of 240 GeV (as in the CEPC), and good sensitivity can in principle be achieved with very high integrated luminosity [29–32]. The simplest diagram is given by the  $\mu\mu t q$  contact term. For the LHC, one recent study be found in ref. [33]. For the MuC the authors in ref. [34] consider  $Q_{lq}^{(1)}$  for the  $\mu\mu tc$  coupling. Other recent studies for FC top couplings at the HL-LHC can be found in [35,36]. We will also consider associated production modes of  $t\bar{u}\gamma$  and  $t\bar{u}Z$  as well as  $\mu^+\mu^- \rightarrow \nu_\mu\nu_\mu t\bar{u}$  where only fermion-boson operators have a potential for good sensitivity.

In order to make an estimate of the potential MuC individual limits for each operator coefficient, let us use a simple criterion: we find the value of the coefficient at which there are a total of one thousand  $t\bar{u} + u\bar{t}$  (that is  $500 + 500$ ) events. Given that there is a different expected luminosity at each energy (see table 1) there are four minimal cross sections depending on the energy. For instance, at  $\sqrt{s} = 3\text{TeV}$  we would have  $\sigma_{\min} = 500\text{ ab}$ .

#### 3.1 Limits on four-fermion operators from $\mu^+\mu^- \rightarrow t\bar{u}$ .

From the cross section result in equation (5) we can obtain the potential limits of the four-fermion coefficients. They are shown in table 2 below.

	3TeV	6TeV	10TeV	14TeV
$10^4 \times  C_{1+3}^{lq-}  \leq$	26.8	6.7	2.5	1.3
$10^4 \times  C_{13}^{lequ1}  \leq$	30.9	7.7	2.9	1.5
$10^4 \times  C_{13}^{lequ3}  \leq$	13.4	3.4	1.3	0.64

Table 2: Limits on the 4-fermion coefficients from  $\mu^+\mu^- \rightarrow t\bar{u}$ .

Notice that we have only included three coefficients in table 2 as the limits of the other five coefficients are the same as seen from eq. (5). These are very stringent limits of order  $10^{-4}$  (for  $\Lambda = 1\text{TeV}$ ). They are three to four orders of magnitude smaller than limits from LHC and LEP data, which are of order 1 [25,37].

#### 3.2 Limits on fermion-boson operators from $\mu^+\mu^- \rightarrow t\bar{u}$ .

For the case of fermion-boson operators we will consider three production modes: first,  $\mu^+\mu^- \rightarrow t\bar{u}$  that involves FCNC couplings only; second, the associated production with an additional  $\gamma$  or  $Z$ ; and third,  $\mu^+\mu^- \rightarrow t\bar{u}\nu_\mu\bar{\nu}_\mu$  that involves diagrams with  $WW$  fusion where FC charged-current couplings may play an important role. We compute the contribution from each operator coefficient, obtain limits on the couplings and compare with the current bounds from the LHC. We compute the tree-level cross section for FC top production at the MuC with the matrix-element Monte Carlo generator MadGraph5.aMC@NLO (henceforth MG5) version 3.5.1 [38]. We implement the dimension-six operators (1) in MG5 by means of FeynRules 2.3.49 [39]. Furthermore, we analyze the events

generated by MG5 with ROOT 6.26 [40]. We also used the program CalcHEP for crosschecks of our results [41]. For the numerical results in this work we use:  $\alpha^{-1} = 127.9$ ,  $\sin^2\theta_W = 0.2337$ ,  $M_Z = 91.187\text{GeV}$ ,  $m_t = 172.5\text{GeV}$ ,  $m_b = 4.5\text{GeV}$ ,  $m_u = m_d = m_s = m_c = 0$  and  $\Lambda = 1\text{TeV}$ .

We will impose the following basic cuts on the transverse momentum and the pseudo-rapidity of the light jet in all the production processes in this section,

$$p_T(j) \geq 10\text{GeV}, \quad |y(j)| \leq 3. \quad (6)$$

The cross sections for  $\mu^+\mu^- \rightarrow t\bar{u}$ , at the energies (3, 6, 10, 14) TeV considered here, and as produced by the operators  $Q_{\varphi u}$  and  $Q_{\varphi q(-)}$ , are actually very low (of order ab):

$$\begin{aligned} \sigma(t\bar{u})/|C_{1+3}^{\varphi q(-)}|^2 &= 120, 30, 11, 6.0 \text{ ab}, \\ \sigma(t\bar{u})/|C_{1+3}^{\varphi u}|^2 &= 30, 7.4, 2.7, 1.4 \text{ ab}. \end{aligned} \quad (7)$$

From the numbers shown in eq. (7) we can already see that the potential limits for operators  $Q_{\varphi q(-)}$  and  $Q_{\varphi u}$  must be higher than 1. Indeed, based on the minimal cross sections required for 1000 ( $t\bar{u} + \bar{t}\bar{u}$ ) events we get  $C_{1+3}^{\varphi q(-)} < 2$  and  $C_{1+3}^{\varphi u} < 4$  at all energies. This sensitivity is about one order of magnitude lower than the current limits reported by ATLAS:  $|C_{1+3}^{\varphi q(-)}|$  and  $|C_{1+3}^{\varphi u}|$  get limits from  $t \rightarrow uZ$  of 0.1 and 0.2 respectively [37] (see appendix B).

In contrast, the cross section  $\sigma(\mu^+\mu^- \rightarrow t\bar{u})$  is large enough for the tensor operators  $Q_{uB}$  and  $Q_{uW}$ . It is constant in energy, and of order fb:

$$\begin{aligned} \sigma(t\bar{u})/|C_{13(31)}^{uB}|^2 &= 75.3 \text{ fb}, \\ \sigma(t\bar{u})/|C_{13(31)}^{uW}|^2 &= 49.4 \text{ fb}. \end{aligned} \quad (8)$$

The reason for such behavior in energy is in the tensor coupling term  $\sigma^{\mu\nu}p_\nu$ . We then will have  $Q_{uB}$  and  $Q_{uW}$  as the two fermion-boson operators with the highest sensitivity for  $\mu^+\mu^- \rightarrow t\bar{u}$ .

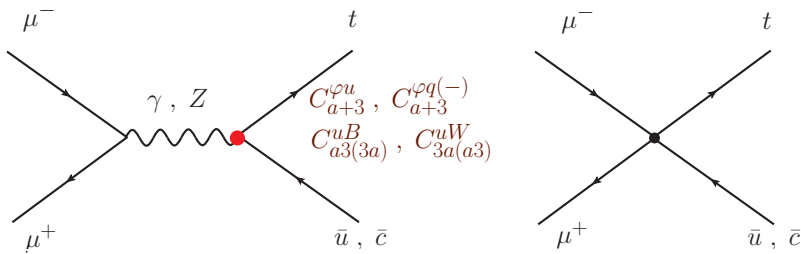


Figure 1: The FC process  $\mu^-\mu^+ \rightarrow t\bar{u}$  ( $\bar{c}$ ) as generated by the  $tq\gamma$  ( $Z$ ) vertex or a  $\mu\mu tq$  contact term.

In table 3 the limits on the coefficients are shown, as obtained from the latest LHC bounds on  $Br(t \rightarrow Vq)$  [37] (see appendix B). We will use the (strongest) bounds from  $t \rightarrow u\gamma$  to compare with the potential limits at the MuC. In table 4 we show the limits we obtain from the minimal cross sections

LHC	$ C_{13(31)}^{uB}  \leq$	$ C_{23(32)}^{uB}  \leq$	$ C_{13(31)}^{uW}  \leq$	$ C_{23(32)}^{uW}  \leq$
$t \rightarrow u\gamma, c\gamma$	0.04	0.08	0.07	0.15
$t \rightarrow uZ, cZ$	0.23	0.34	0.13	0.19

Table 3: Limits on  $|C^{uB}|$  and  $|C^{uW}|$  from LHC top decay measurements [37].

required for 500  $t\bar{u}$  events. We are showing the ratios  $R = |C_{\mu\text{MuC}}^{\max}|/|C_{\text{LHC}}^{\max}|$  to establish the comparison. At the higher energies 10, 14 TeV the constraints are stronger by a factor of 2 or 3.

	3TeV	6TeV	10TeV	14TeV
$10^2 \times  C_{13(31)}^{uB}  \leq$	8.9 ( $R = 2.1$ )	4.4 ( $R = 1.0$ )	2.0 ( $R = 0.65$ )	1.4 ( $R = 0.45$ )
$10^2 \times  C_{13(31)}^{uW}  \leq$	11 ( $R = 1.4$ )	5.5 ( $R = 0.72$ )	2.5 ( $R = 0.46$ )	1.7 ( $R = 0.32$ )

Table 4: Limits on the coefficients from  $\mu^- \mu^+ \rightarrow t\bar{u}$ . The ratios  $R = |C_{\mu\text{MuC}}^{\max}| / |C_{\text{LHC}}^{\max}|$  are shown.

Let us notice that in obtaining the results of equations (7) and (8) we have ignored contributions from the SM. Because of the GIM mechanism [42] there are no FCNC couplings in the SM at tree level. At the one loop level the mechanism does not quite hold because of the difference in up type quark masses. If the masses  $m_u$ ,  $m_c$  and  $m_t$  were equal there would be no FCNC couplings either (see for instance [43]). The decay  $b \rightarrow s\gamma$  (or  $b \rightarrow d\gamma$ ) is sizeable enough to be observable because of the size of the top quark mass. However, the decay  $t \rightarrow u\gamma$  (or  $t \rightarrow c\gamma$ ) is very small, of order  $10^{-13}$  because  $m_b$  is large compared to  $m_s$  and  $m_d$  but still much smaller than  $m_t$ . To give us an idea of how large is the SM contribution to the Wilson coefficients let us take a look at the branching ratios [22]:

$$Br(t \rightarrow uV) = f_Q \times 10^{-3} |C_{13,31}^Q|^2 .$$

With  $f_Q \simeq (0.5, 11)$  for  $V = (H, G)$  and  $Q = (Q_{u\varphi}, Q_{uG})$ ;  $f_Q \simeq (2.0, 6.4)$  for  $V = \gamma$  and  $Q = Q_{uW}, Q_{uB}$ ;  $f_Q \simeq (6.7, 1.7, 3.8, 1.2)$  for  $V = Z$  and  $Q = Q_{\varphi q(-)}, Q_{\varphi u}, Q_{uW}, Q_{uB}$ . So we see that  $B_{\text{SM}}(t \rightarrow u\gamma) \sim 10^{-13}$  means that the SM contribution to the coefficients is of order  $10^{-5}$ . This number is at least three orders of magnitude smaller than the potential MuC limits we are obtaining. The SM contribution is negligible.

### 3.3 Associated production $\mu^- \mu^+ \rightarrow t\bar{u}V$ , with $V = \gamma, Z, g$ .

Let us now consider the associated production modes  $t\bar{u}\gamma$  and  $t\bar{u}Z$  that involve  $\mu^+ \mu^-$  annihilation. In fig. 2 we show three sample diagrams. Notice that the FC coupling can appear in the internal line as in  $t\bar{u}$  production and then the  $\gamma$  or  $Z$  boson is emitted via the regular SM coupling. There is another source of flavor change when the photon (or  $Z$ ) is emitted via the dimension six operator. For the tensor operators the coupling is proportional to the energy of the  $\gamma$  or  $Z$  and we expect some effect of increasing amplitude values as the energy of the collider is also increased.

For  $t\bar{u}\gamma$  we impose, in addition to eq. (6), the following cuts:

$$p_T(\gamma) \geq 10\text{GeV} , |y(\gamma)| \leq 3 , \Delta R(\gamma, j) \geq 0.4 . \quad (9)$$

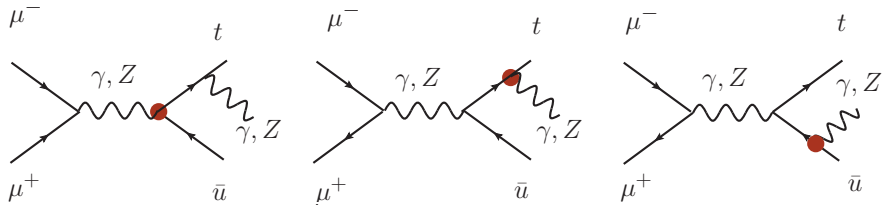


Figure 2: The FC process  $\mu^- \mu^+ \rightarrow t\bar{u} + \gamma(Z)$ . The FC coupling involves either the internal or the external boson line.

As in the case of  $t\bar{u}$  production, the cross section numbers produced by the operators  $Q_{\varphi u}$  and  $Q_{\varphi q(-)}$  are rather low:

$$\begin{aligned} \sigma(t\bar{u}\gamma[t\bar{u}Z]) / |C_{1+3}^{\varphi q(-)}|^2 &= 20 [160], 6.6 [44], 2.8 [17], 1.6 [7.0] \text{ ab}, \\ \sigma(t\bar{u}\gamma[t\bar{u}Z]) / |C_{1+3}^{\varphi u}|^2 &= 5.8 [36], 1.8 [9.5], 0.74 [3.6], 0.42 [1.9] \text{ ab}. \end{aligned} \quad (10)$$

Again, the coefficients would have to take on values of about 10 in order to produce enough events in  $t\bar{u}\gamma$  and of about 4 or 5 in  $t\bar{u}Z$  production. We conclude that, as before, the MuC has a low sensitivity for  $Q_{\varphi u}$  and  $Q_{\varphi q(-)}$  in this case.

For operators  $Q_{uB}$  and  $Q_{uW}$  the cross sections produced are:

$$\begin{aligned}\sigma(t\bar{u}\gamma[t\bar{u}Z])/|C_{13(31)}^{uB}|^2 &= 10 [18], 12 [70], 14 [197], 15 [385] \text{ fb}, \\ \sigma(t\bar{u}\gamma[t\bar{u}Z])/|C_{13(31)}^{uW}|^2 &= 6.5 [12], 8.2 [46], 9.3 [129], 10 [252] \text{ fb}.\end{aligned}\quad (11)$$

To set limits we now require the minimal cross sections to be twice the values requested before, that is 2000 events ( $t\bar{u} + \bar{t}u$ ). The reason is that we expect the background to significantly increase when considering the emission of a photon, and even more so when considering the two additional fermions from  $Z$  decay.

In table 5 we show the limits associated with these production modes. If we compare with the limits from  $t\bar{u}$  in table 4, we can see that the limits are now weaker coming from  $t\bar{u}\gamma$  and are of similar size when coming from  $t\bar{u}Z$ . Of course, these are rough estimates but we believe that  $t\bar{u}\gamma$  and  $t\bar{u}Z$  production could be useful in a global analysis because four-fermion operators should yield a lower cross section in this mode. The emission of  $\gamma, Z$  with four-fermion couplings must come from regular SM couplings.

Another operator with low sensitivity is  $Q_{uG}$ . The only process at the MuC at tree level to be considered is the radiative associated production of single top:  $\mu^+\mu^- \rightarrow t\bar{u}g$ . We have computed the cross sections at the energies of table 1, with  $C_{13(31)}^{uG} = 1$  and applying some basic cuts to avoid soft and collinear regions, as in  $t\bar{u}\gamma$ , with the result of a constant  $\sigma(\mu^+\mu^- \rightarrow t\bar{u}g) = 62 \text{ ab}$  for the entire range of energies  $\sqrt{s} = 3 - 14 \text{ TeV}$ . The energy dependence of the tensor coupling is proportional to  $\sqrt{s}$  and that is the reason why the cross section remains essentially constant with increasing energy. This small value for the cross section suggests a sensitivity to  $C_{13(31)}^{uG}$  somewhat higher than of order 1. This is much lower than the current limits obtained at the LHC. Indeed,  $Q_{uG}$  is very well probed with the single top quark production  $gu(gc) \rightarrow t$  as well as the decay process  $t \rightarrow ug(cg)$  at the LHC. The current limits from non observation of  $t \rightarrow ug(cg)$  decay as reported by ATLAS are  $|C_{13(31)}^{uG}| \leq 0.074$  and  $|C_{23(32)}^{uG}| \leq 0.18$  [37] (see appendix B). We remark, however, that  $Q_{uG}$  may still play an important role in a lepton collider study in the framework of a global analysis involving QCD NLO corrections [25].

	3TeV	6TeV	10TeV	14TeV
$t\bar{u}\gamma: 10^2 \times  C_{13(31)}^{uB}  \leq$	32 ( $R = 8.0$ )	15 ( $R = 3.8$ )	8.4 ( $R = 2.1$ )	5.8 ( $R = 1.5$ )
$t\bar{u}Z:$	24 ( $R = 6.0$ )	6.0 ( $R = 1.5$ )	2.3 ( $R = 0.58$ )	1.2 ( $R = 0.3$ )
$t\bar{u}\gamma: 10^2 \times  C_{13(31)}^{uW}  \leq$	39 ( $R = 5.6$ )	18 ( $R = 2.6$ )	10 ( $R = 1.4$ )	7.1 ( $R = 1.0$ )
$t\bar{u}Z:$	29 ( $R = 4.1$ )	7.4 ( $R = 1.1$ )	2.8 ( $R = 0.4$ )	1.4 ( $R = 0.2$ )

Table 5: Limits on the coefficients from  $\mu^-\mu^+ \rightarrow t\bar{u}V$  with  $V = \gamma, Z$  obtained with the minimal cross sections required for 1000  $t\bar{u}$  events.

### 3.4 The process $\mu^-\mu^+ \rightarrow t\bar{u}\nu_\mu\bar{\nu}_\mu$ .

This process offers a richer phenomenology than the previous  $t\bar{u}$  or  $t\bar{u}\gamma(Z)$ . In the SM, one can have the three t-channel  $WW$  fusion diagrams like the one in the left hand side of fig. 3. When we add them together, they cancel each other. This is due to the unitarity of the CKM matrix –the GIM mechanism. Therefore, the SM contribution is zero at tree level. When we include the dimension six FC couplings like  $Wtd$  or  $Wub$  there is no more cancellation and we can get a non-zero cross section. At high energies the contribution from these  $WW$  fusion diagrams becomes significant or even dominant, and then a computational simplification can be used, known as the effective  $W$  approximation (EWA) [3, 44].

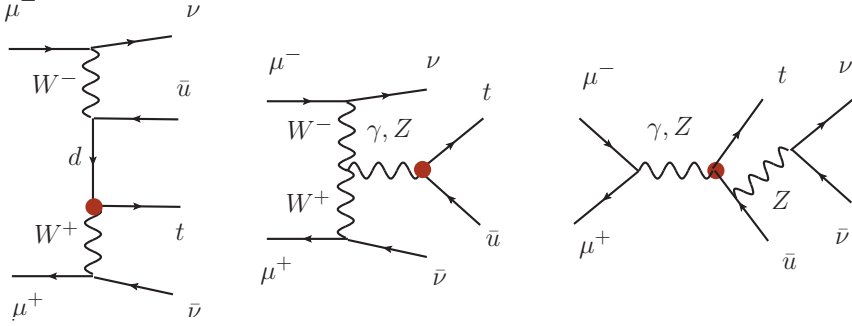


Figure 3: The FC process  $\mu^- \mu^+ \rightarrow t\bar{u} \nu\bar{\nu}$ : three sample diagrams.

Let us focus on these t-channel  $WW$  fusion diagrams without the leptonic lines as presented in fig. 4 where the coefficient associated to each effective coupling is shown for clarity. We are not making use of the EWA in our calculations but it is instructive to see what happens when we compute the two-to-two amplitudes of fig. 4. Regarding the CKM matrix elements, it is known that the third family subleading flavor mixing elements are very small, of order  $10^{-2}$  or less. We have performed several of the calculations keeping all the CKM elements, and then we have made the assumption  $V_{ts} = V_{td} = V_{ub} = V_{cb} = 0$  and  $V_{tb} = 1$ . As expected, we have found that the numerical results are essentially the same. From now on, we will make our discussion bearing in mind this (Cabbibo matrix) simplification. In (12) we show the cross section for  $W^+W^- \rightarrow t\bar{u}$  using the contribution of each operator coefficient separately. They are given for three sample energies  $\sqrt{s} = 1, 2, 4$  TeV and we are writing them in ascending order:

$$\begin{aligned}
\sigma_{ww}/|C_{13}^{\varphi ud}|^2 &= 40, 29, 27 \text{ ab.} \\
\sigma_{ww}/|C_{13}^{dW}|^2 &= 520, 430, 410 \text{ ab.} \\
\sigma_{ww}/|C_{13(31)}^{uB}|^2 &= 3.7, 3.4, 3.3 \text{ fb.} \\
\sigma_{ww}/|C_{13(31)}^{u\varphi}|^2 &= 75, 77, 78 \text{ fb.} \\
\sigma_{ww}/|C_{1+3}^{\varphi q(-)}|^2 &= 400, 330, 310 \text{ fb.} \\
\sigma_{ww}/|C_{1+3}^{\varphi u}|^2 &= 1.9, 7.1, 28 \text{ pb.} \\
\sigma_{ww}/|C_{1+3}^{\varphi q(+)}|^2 &= 8.0, 28, 110 \text{ pb.} \\
\sigma_{ww}/|C_{13(31)}^{uW}|^2 &= 9.0, 29, 112 \text{ pb.}
\end{aligned} \tag{12}$$

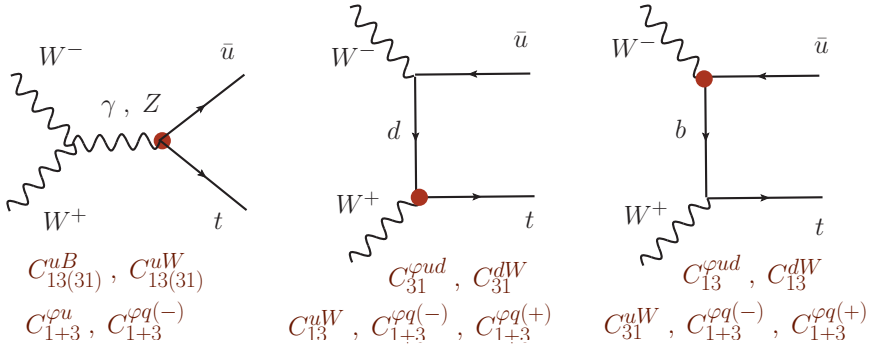


Figure 4: The  $WW$  fusion processes  $W^-W^+ \rightarrow t\bar{u}$ : s-channel and t-channel diagrams.

The first line in (12) shows the results for operator  $Q_{\varphi ud}$ . It turns out that  $C_{31}^{\varphi ud}$  yields a cross section equal to zero. This is because of a chirality flip on the  $d$ -quark line causing the amplitude to be

proportional to  $m_d$ . On the other hand,  $C_{13}^{\varphi ud}$  refers to a diagram with a  $b$ -quark propagator and the amplitude is now proportional to  $m_b$  (4.5 GeV). A similar situation occurs with the operator  $Q_{dW}$ .

The third smallest  $WW$  fusion cross section in (12) comes from the tensor operator  $Q_{uB}$ . This can be regarded as a surprise because the couplings of tensor operators are proportional to the gauge boson momentum. Indeed, let us be reminded that the operator with the highest  $\mu^+ \mu^- \rightarrow t\bar{t}$  cross section is precisely  $Q_{uB}$ . What happens in  $W^+ W^- \rightarrow t\bar{t}$  is that there is a destructive interference between the two diagrams: the one with a photon and the one with a  $Z$  propagator. Nevertheless, when we compute the cross section of the full  $\mu^- \mu^+ \rightarrow t\bar{t}\nu_\mu \bar{\nu}_\mu$  process we find out that  $Q_{uB}$  actually yields the second highest cross section. The explanation is that the  $WW$  fusion diagrams are not significant for  $Q_{uB}$ . The other diagrams are providing all the total cross section. As shown in fig. 3, they can be viewed as  $\mu^+ \mu^-$  annihilation into  $t\bar{t}$  plus the emission of a neutrino pair from any of the fermion lines.

About the inclusion of  $Q_{\varphi q(+)}$ , we should bear in mind that this operator generates FCNC  $Zbu$  and  $Zbs$  couplings that can be strongly constrained by  $B$  meson measurements. However, a global analysis in the future may take into account the potential contribution of  $Q_{\varphi q(+)}$  to the single top-quark production process. After all, in our list of cross sections,  $Q_{\varphi q(+)}$  yields the second highest numbers. Remarkably, it is in fact almost identical to the yield of  $Q_{uW}$ .

Concerning the validity of eq. (12) as far as unitarity violation is concerned, we point out that, the limits on the coefficients that we obtain in tables 7 and 8 are well below the unitarity limits. In particular, we find from ref. [45] that the bounds are given by  $|C_Q s/\Lambda^2| < 28, 111, 14, 34$  for  $C_Q = C_{13}^{uW}, C_{13}^{uB}, C_{1+3}^{\varphi q\pm}, C_{1+3}^{\varphi u}$  respectively ( $\Lambda = 1$  TeV,  $\sqrt{s} = 1, 2, 4$  TeV).

Now let us go ahead with the discussion of the process of interest. In eq. (13) we show the cross section of  $\mu^- \mu^+ \rightarrow t\bar{t}\nu_\mu \bar{\nu}_\mu$  for each operator coefficient separately. They are given for the four energies of table 1 and we are writing them again in ascending order:

$$\begin{aligned}
\sigma/|C_{13}^{\varphi ud}|^2 &= 0.016, 0.032, 0.047, 0.058 \text{ ab.} \\
\sigma/|C_{13}^{dW}|^2 &= 0.31, 0.76, 1.3, 1.8 \text{ ab.} \\
\sigma/|C_{13(31)}^{u\varphi}|^2 &= 18, 38, 58, 74 \text{ ab.} \\
\sigma/|C_{1+3}^{\varphi q(-)}|^2 &= 0.09, 0.19, 0.29, 0.37 \text{ fb.} \\
\sigma/|C_{1+3}^{\varphi u}|^2 &= 0.19, 0.86, 2.5, 5.0 \text{ fb.} \\
\sigma/|C_{1+3}^{\varphi q(+)}|^2 &= 0.67, 3.0, 8.8, 17 \text{ fb.} \\
\sigma/|C_{13(31)}^{uB}|^2 &= 1.2, 4.6, 13, 25 \text{ fb.} \\
\sigma/|C_{13(31)}^{uW}|^2 &= 4.0, 21, 69, 147 \text{ fb.}
\end{aligned} \tag{13}$$

The operators  $Q_{\varphi ud}$  and  $Q_{dW}$  yield remarkably small cross sections, showing that these are indeed low-sensitivity operators. Moreover, their coefficients get very strong limits, of order less than  $10^{-2}$ , from  $B$  meson decays and  $pp \rightarrow \ell\nu$  at the LHC [14, 46]. These operators can therefore be ignored in processes based on top production at the MuC.

In the third place we have  $Q_{u\varphi}$ . This operator belongs to the group that only generates couplings with the top quark, so we do not expect any strong constraints from  $B$  measurements. The current limits from non observation of  $t \rightarrow uH$  and  $t \rightarrow cH$  decays at the LHC as reported by ATLAS are  $|C_{13(31)}^{u\varphi}| \leq 0.96$  and  $|C_{23(32)}^{u\varphi}| \leq 1.1$  [47]. In principle, we can imagine that Higgs associated production  $\mu^+ \mu^- \rightarrow t\bar{t}H$  may be a good probe for this coupling. However, we have obtained cross sections of order  $10^{-1}$  ab or less at all energies (with coefficient equal to 1). For  $t\bar{t}\nu_\mu \bar{\nu}_\mu$  production we obtain not as small cross section numbers, but they may not be enough to get limits of order 1. Therefore, the sensitivity for  $C_{13(31)}^{u\varphi}$  at the MuC is likely to be somewhat weaker than the current constraints from the LHC. In any case, associated production of top and Higgs may still be an important measurement at the MuC, in a recent article the authors show that CP violating effects of the top Yukawa coupling

$t\bar{t}H$  may be probed through  $t\bar{t}H$  production mode [48].

Regarding the other six operators, when computing the amplitude for  $\mu^-\mu^+ \rightarrow t\bar{t}\nu_\mu\bar{\nu}_\mu$  it turns out that one gets many more possible diagrams than in the associated  $t\bar{t}\gamma(Z)$  production. Specifically, for  $Q_{\varphi u}$  and  $Q_{\varphi q(-)}$  we obtain 15 diagrams. For  $Q_{uB}$  we obtain 22 and for  $Q_{uW}$  there are 26. When we consider  $Q_{\varphi u}$  or  $Q_{\varphi q(-)}$  the s-channel  $WW$  fusion diagrams only involve the effective  $t\bar{t}Z$  vector coupling.

As noted in the previous section  $Q_{\varphi q(+)}$  and  $Q_{\varphi q(-)}$  generate a  $Wub$  coupling which can be probed with the  $b \rightarrow u\ell\nu$  decay for example. In fact, very strong limits: of order  $2 \times 10^{-3}$ , have been reported in a recent article [14]. In addition, there are also much weaker limits from the non-observation of  $t \rightarrow uZ(cZ)$  decay at the LHC as reported by ATLAS [37]:  $|C_{1+3}^{\varphi q(-)}| \leq 0.10$  and  $|C_{2+3}^{\varphi q(-)}| \leq 0.14$  (see appendix B). We point out that similar limits on  $|C_{a+3}^{\varphi q(-)}|$  can be found in ref. [25], where they also used  $tj$  production at LEP data. A surprising result in eq. (13) is that it is actually  $Q_{\varphi q(+)}$ , not  $Q_{\varphi q(-)}$ , the operator that gives a greater cross section for  $t\bar{t}\nu_\mu\bar{\nu}_\mu$  production. In any case, we should bear in mind that both of them receive very strong limits from  $B$  measurements.

The fact that, except for  $Q_{uB}$ , the same ranking that we observe in eq. (12) appears again in eq. (13) points toward the significance of  $WW$  fusion in the production processes of a high energy MuC. It is because of this feature of a high energy MuC, that it has been dubbed as a virtual *gauge boson collider* [3]. However, and contrary to this statement, there may be processes where the  $WW$  fusion diagrams are not so significant even at high energies. The reason why  $Q_{uB}$  yields such high rates in the full process is because there are 20 other diagrams, like the ones on the right-side of fig. 3 that involve FCNC  $\gamma tu$  and  $Ztu$  couplings. They grow with energy and there is apparently no cancellation taking place between them. None of them correspond to a gauge boson fusion process. As a confirmation that our reasoning is correct we will now turn our attention to another  $t\bar{t}$  plus neutrinos production process: one where the neutrinos are not the  $SU(2)$  partners of the muon. In this process there cannot be any  $WW$  fusion diagram. It turns out that the cross section for  $Q_{uB}$  when we substitute  $\nu_\mu$  for  $\nu_e$  or  $\nu_\tau$  is almost exactly the same. The same does not happen with  $Q_{uW}$ , for which the contribution from the other neutrino final states is small. Below, we give the cross section for these additional modes: With

$\sigma(fb)$	3TeV	6TeV	10TeV	14TeV
$C_{13(31)}^{uB}$	$\nu_e + \nu_\tau$	2.3	9.3	26
	$\nu_e + \nu_\mu + \nu_\tau$	3.5	14	39
$C_{13(31)}^{uW}$	$\nu_e + \nu_\tau$	1.5	6.1	17
	$\nu_e + \nu_\mu + \nu_\tau$	5.6	27	75
				180

Table 6: Cross sections  $\sigma(\mu^-\mu^+ \rightarrow t\bar{q}\nu\bar{\nu})(fb)$  for the modes  $\nu = \nu_e, \nu_\tau$ . The sum of the three modes  $\nu = \nu_e, \nu_\mu, \nu_\tau$  is also shown.

the total cross sections shown in table 6 we now make an estimate on the sensitivity from  $\mu^-\mu^+ \rightarrow t\bar{t}\nu\bar{\nu}$  at the MuC for the operators of our main interest in this study. We are assuming that 5% of the signal events will pass the cuts and request a value of the coefficient necessary for 25 events. In table 7 we show the limits for  $C_{13(31)}^{uB}$  and  $C_{13(31)}^{uW}$ . We also show the ratio with respect to the current ATLAS limits presented in table 3. We notice that at the highest energies the MuC may provide bounds two to four times more stringent than what the LHC has obtained from the most sensitive probe that is  $t \rightarrow u\gamma$  decay. In the following section we will perform a more in-depth study of the limits for  $C_{13,31}^{uW,uB}$  by considering the decay products of top quark in the hadronic channel.

To end this section, in table 8 we also show the limits obtained for the other couplings. For  $C_{13(31)}^{\varphi\varphi}$  we notice that the MuC could only provide similar bounds to the FCNC top-Higgs couplings that the LHC has already achieved. Concerning  $C_{13(31)}^{\varphi q(-)}$  the current LHC bounds from  $t \rightarrow uZ$  are 0.1 which

	3TeV	6TeV	10TeV	14TeV
$10^2 \times  C_{13(31)}^{uB}  \leq$	54 ( $R = 14$ )	13 ( $R = 3.4$ )	5.1 ( $R = 1.3$ )	2.6 ( $R = 0.65$ )
$10^2 \times  C_{13(31)}^{uW}  \leq$	42 ( $R = 6.0$ )	9.6 ( $R = 1.4$ )	3.7 ( $R = 0.53$ )	1.7 ( $R = 0.24$ )

Table 7: Limits on the coefficients from  $\mu^- \mu^+ \rightarrow t\bar{t}\nu\nu\bar{\nu}$  obtained with the minimal cross sections required for 1000  $t\bar{t}$  events. The ratios  $R = |C_{\mu\text{MuC}}^{\max}|/|C_{\text{LHC}}^{\max}|$  are shown.

is already twice as strong as the lowest limit in table 8. We also show limits for  $C_{13(31)}^{\varphi q(+)}$  even though an FC bottom quark production would likely be the best process to use as probe of this operator. In any case, we think it is worth noting that even single top production could be a somewhat sensitive measurement. To underline the importance of the limits shown in table 8 we point out that there are models that give rise to tree level contributions to vector operators like  $Q_{\varphi q(\pm)}$  and  $Q_{\varphi u}$  but only loop level contributions to the tensor operators in table 7 [49].

	3TeV	6TeV	10TeV	14TeV
$ C_{13(31)}^{u\varphi}  \leq$	7.5 ( $R = 6.2$ )	2.6 ( $R = 2.2$ )	1.3 ( $R = 1.1$ )	0.82 ( $R = 0.69$ )
$ C_{1+3}^{\varphi u}  \leq$	2.3 ( $R = 12$ )	0.54 ( $R = 2.8$ )	0.20 ( $R = 1.1$ )	0.10 ( $R = 0.53$ )
$ C_{1+3}^{\varphi q(-)}  \leq$	3.3 ( $R = 33$ )	1.2 ( $R = 12$ )	0.59 ( $R = 5.9$ )	0.37 ( $R = 3.7$ )
$ C_{1+3}^{\varphi q(+)}  \leq$	1.2 ( $R = 600$ )	0.29 ( $R = 145$ )	0.11 ( $R = 55$ )	0.054 ( $R = 27$ )

Table 8: Limits on the coefficients from  $\mu^- \mu^+ \rightarrow t\bar{t}\nu\mu\bar{\nu}_\mu$  obtained with the minimal cross sections required for 1000  $t\bar{t}$  events. For the ratio  $R$  of  $C_{1+3}^{\varphi q(+)}$  we use the limit of  $2 \times 10^{-3}$  from  $B$ -meson decays [14].

## 4 Limits on $|C_{k3,3k}^{uW}|$ and $|C_{k3,3k}^{uB}|$ from $t\bar{q}_u\nu\bar{\nu}$ production in hadronic channel.

In this section we consider the single-top production process discussed in section 3.4 in the hadronic decay channel which, at the parton level, leads to six-fermion final states,

$$\mu^+ \mu^- \rightarrow t\bar{q}_u\nu\bar{\nu} + \bar{t}q_u\nu\bar{\nu} \rightarrow b q_u \bar{q}_d \bar{q}_u \nu\bar{\nu} + \bar{b} \bar{q}_u q_d q_u \nu\bar{\nu}, \quad \text{with } q_u = u, c, q_d = d, s, \nu = \nu_e, \nu_\mu, \nu_\tau. \quad (14)$$

This equation defines our parton-level signal process, which is not allowed in the SM at tree level and must proceed, therefore, through effective FC couplings. We simulate the signal process and its SM backgrounds in the unitary-gauge SM, with two massless generations, with Cabibbo mixing in the quark sector, augmented by the dimension-6 operators (1). As mentioned above, we implement those operators in MG5 [38] with FeynRules [39], and analyze the MG5 events with ROOT [40].

Representative Feynman diagrams for (14) can be obtained by attaching appropriate hadronic decay vertices to the top lines in figure (3). We let  $C_{13}^{uW} \neq 0 \neq C_{31}^{uW}$  and  $C_{13}^{uB} \neq 0 \neq C_{31}^{uB}$  one at a time, and set all other Wilson couplings to vanish. For each Wilson coefficient there are diagrams containing  $n$  effective vertices, with  $1 \leq n \leq 4$ . In practice, however, for  $|C_{ij}^{uW,uB}| \lesssim 1$ , only diagrams with one anomalous vertex are numerically significant. Those diagrams involve the off-diagonal couplings  $C_{k3,3k}^{uW,uB}$  with  $k = 1, 2$ . In the remainder of this section we refer to  $C_{13,31}^{uW,uB}$  for concreteness, in the understanding that the results obtained apply equally well to  $C_{23,32}^{uW,uB}$ .

Besides the signal process (14), we take into account several SM backgrounds with four partons and one or more neutrinos in the final state. In what follows, we focus on the most resonant processes. SM

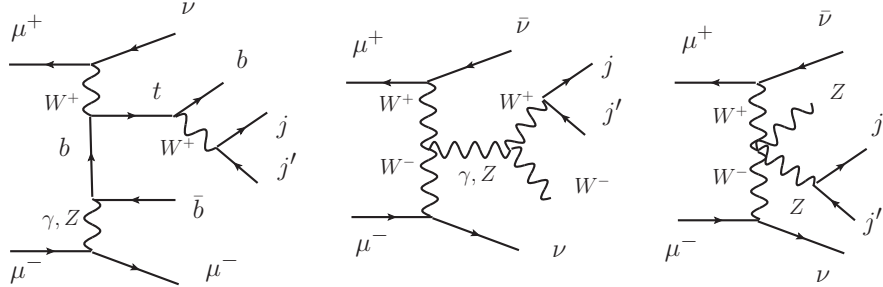


Figure 5: The background processes: single top,  $Zjj$  and  $Wjj$  production, some sample diagrams.

$t\bar{t}$  production through  $\mu^+\mu^-$  annihilation, with one top decaying hadronically according to the SM, and the other via an effective FC coupling as  $t \rightarrow q_u Z \rightarrow q_u \nu \bar{\nu}$ , leads to the same final states as in (14). The cross section for this process, however, is negligibly small compared to that of the signal process, so we will not dwell further on it. Similarly, we consider triply resonant  $W^+W^-Z$  and  $ZZZ$  production, with two bosons decaying hadronically and one  $Z \rightarrow \nu \bar{\nu}$ . These processes also have negligibly small cross sections, so we ignore them in what follows.

We considered also doubly-resonant production of  $WW$ ,  $WZ$  and  $ZZ$  vector bosons. Out of those, only the first one yields a large enough cross section to merit further discussion. A Feynman diagram for the production of  $WW$  in a vector-boson fusion (henceforth VBF) process is shown in figure 5. Other topologies, such as  $\mu^+\mu^-$  annihilation, are not shown for brevity. This  $WW$  background can be associated with any of the three neutrino flavors, but it is only the process with  $\nu = \nu_\mu$ , which is the only one containing the VBF diagrams, that gives a numerically significant contribution. As can be seen in the figure, this is a reducible background, with no  $b$  quark in the final state. Numerical results for this  $WW$  background cross section are given below in table 9 under the label “ $WW$ .”

Singly resonant  $Wjj$  production is another important reducible background process. A Feynman diagram for this process is given by the  $WW$  diagram in figure 5, with one of the  $W$  bosons on-shell and the other one off-shell. As with  $WW$  production, only the diagrams with  $\nu = \nu_\mu$  of the VBF type are numerically relevant. Numerical results for the cross sections for this background are given below in table 9 with the label “ $Wjj$ .” Another important singly-resonant background is  $Zjj$  production. The diagrams containing the decay  $Z \rightarrow q\bar{q}$ , with  $q$  any quark flavor including  $q = b$ , and  $\nu = \nu_\mu$  are the diagrams that give the only numerically relevant contribution to the single- $Z$  production cross section. Numerical results for the cross section for this background are given below in table 9 under the label “ $Zjj$ .”

We consider, finally, SM top production in  $\mu^+\mu^-$  collisions. Top-pair production from  $\mu^+\mu^-$  annihilation, in semileptonic mode, with the charged lepton outside the central region, is a reducible background. Its cross section is very small, however, so we do not consider it further. Top-pair production of the form  $\mu^+\mu^- \rightarrow t\bar{t}\nu\bar{\nu}$ , which contains  $t\bar{t}$  production in VBF among other processes, is also a reducible background in semileptonic mode with the charged lepton outside the central region. Its cross section is larger than that of the annihilation process, but still negligibly small. The main SM top-production background at high energies is single-top production in association with a  $b$  jet,

$$\mu^+\mu^- \rightarrow t\bar{b}\ell^-\nu_\ell + \bar{t}b\ell^+\bar{\nu}_\ell \rightarrow b q_u \bar{q}_d \bar{b}\ell^-\nu_\ell + \bar{b}\bar{q}_u q_d b\ell^+\bar{\nu}_\ell. \quad (15)$$

This process is given by  $t$  (or  $\bar{t}$ ) production with  $\ell$  any of the three charged leptons, but again only the processes with  $\ell = \mu$  lead to a substantial cross section. Among those, only the VBF processes are significant. It is illustrated by the leftmost diagram in figure 5. Single-top production has two  $b$  quarks in the final state, and is therefore a reducible background. Numerical results for its cross section are given below in table 9 with the label “ $tb$ .”

We carry out the event selection of our simulated signal and background events by means of a set of phase-space cuts. We consider final states with four partons, which we interpret as “jets,” and transverse missing energy. We denote the jets  $J_{0,\dots,3}$ , ordered by decreasing  $p_T$ . We then select events satisfying the phase-space cuts,

$$\begin{aligned} p_T(J_0) &\geq \dots \geq p_T(J_3) > 30 \text{ GeV}, & \cancel{E}_T &> 50 \text{ GeV}, & |y(J_{0,\dots,3})| &< 3, \\ \Delta R(J_a, J_b) &> 0.4, & m(J_a, J_b) &> 20 \text{ GeV}, & a \neq b &= 0, \dots, 3, \end{aligned} \quad (16)$$

where  $p_T = |\vec{p}_T^\perp|$  is the transverse momentum,  $\cancel{E}_T = |\vec{p}_\nu^\perp + \vec{p}_{\bar{\nu}}^\perp|$  is the missing transverse energy, and  $\Delta R = \sqrt{(\Delta y)^2 + (\Delta\varphi)^2}$ . The purpose of the cuts (16) is fourfold: (i) to ensure that the jets are in the central region where  $b$ -tagging is operational and efficient, (ii) to ensure good numerical convergence of the simulation algorithms, (iii) to suppress background processes, whose jets tend to be somewhat softer than those in the signal processes, and (iv) to select events with well separated partons in the final state, which are the parton-level idealization of four-jet events at the detector level. This last point deserves further consideration. At the extremely high energies the muon collider is foreseen to reach, we can expect events with highly boosted top quarks resulting in fewer and fatter jets in the final state. This is indeed the case in two-body reactions of the form  $\mu^+ \mu^- \rightarrow t\bar{q}_u + \bar{t}q_u$  [34]. For processes with additional leptons in the final state, and in particular for VBF processes, however, a significant portion of the cross section is provided by four-jet events. This is illustrated by the differential cross sections shown in figure 6. In this preliminary study, we focus our analysis precisely on those four-jet events, which are enough to attain substantial sensitivity to the effective flavor off-diagonal couplings  $C_{13,31}^{uW}$  and  $C_{13,31}^{uB}$ , as shown below.

Each jet is assigned a  $b$ -tag, for which purpose we adopt a working point with a  $b$ -tagging efficiency  $\eta_b = 0.85$ , and mistagging probabilities  $p_c = 0.10$  for  $c$ -jets and  $p_j = 0.01$  for lighter jets. Our event selection is further refined by requiring the same number of  $b$ -tagged and light jets as in (14),

$$N_b = 1, \quad N_j = 3. \quad (17)$$

For events satisfying (17), we designate the  $b$ -tagged jet as  $J_b$ . We construct the mass differences  $\Delta m = |m(j, j') - m_W|$ , for non- $b$  tagged jets  $j, j'$ , and identify the pair of jets minimizing  $\Delta m$  as the  $W$  decay products. We denote those jets as  $J_{q0}, J_{q1}$ , ordered by  $p_T$ . The remaining light jet is identified as the light “spectator” jet produced in the effective FC coupling, and denoted  $J_{\text{spt}}$ . We then require the events to satisfy the mass cuts

$$|m(J_{q0}, J_{q1}) - m_W| < 30 \text{ GeV}, \quad |m(J_b, J_{q0}, J_{q1}) - m_t| < 30 \text{ GeV}, \quad (18)$$

where  $m_W = 80.377$  GeV,  $m_t = 172.69$  GeV [50]. In figure 6 we show the distribution of the transverse momentum of, and the phase-space distance between, the four final-state jets. As seen there, there is a substantial fraction of events where the final-state particles are well separated. Finally, in the case of SM top production, as discussed above, we require the final-state charged lepton to be outside the central region,

$$\text{SM : } |y(\ell^\pm)| > 3. \quad (19)$$

With the set of cuts described above, we obtain the cross sections for the signal and background processes. The results are summarized in table 9, where the cross sections for the signal process (14) are given for the effective FC couplings  $C_{13,31}^{uW}$  and  $C_{13,31}^{uB}$  taken non-zero one at a time.

As expected by the total cross sections in eq. (13), we observe here that the signal cross sections for  $C_{13,31}^{uW} \neq 0$ , with cuts, grow with  $\sqrt{s}$ . This reflects both, the dominating contribution of VBF for these couplings, and the fact that a significant fraction of events contains well separated final-state particles satisfying (16). For  $C_{13,31}^{uB}$ , we notice in eq. (13) that the growth in energy is slower and then, after

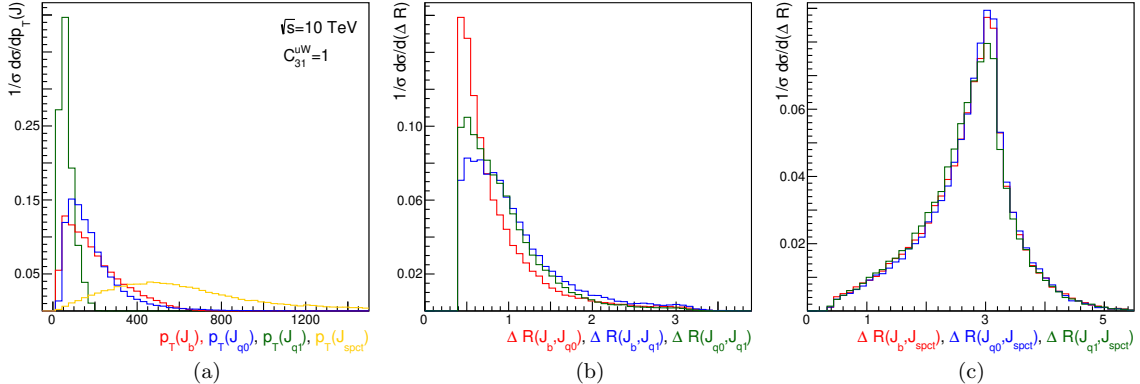


Figure 6: Differential cross sections for the signal process (14), at  $\sqrt{s} = 10$  TeV and for  $C_{31}^{uW} = 1$  and all other effective FC couplings vanishing, with respect to (a) the transverse momentum of the top decay products  $J_b$ ,  $J_{q0}$ ,  $J_{q1}$ , and the spectator jet  $J_{\text{spect}}$ , (b) the  $\Delta R$  distance between top decay products, (c) the  $\Delta R$  distance between top decay products and the spectator jet.

imposing the cuts, the growth disappears. This reflects the fact that the VBF process is not dominant for this coupling.

Also important are the results shown in table 9 for the main background processes, as described above.

$\sqrt{s}$ [TeV]	$\sigma$ [fb]			
	3	6	10	14
$\sigma_{d6}/ C_{13}^{uW} ^2$	1.254	2.568	3.709	4.446
$\sigma_{d6}/ C_{31}^{uW} ^2$	1.382	3.097	4.687	5.716
$\sigma_{d6}/ C_{13}^{uB} ^2$	0.418	0.412	0.364	0.308
$\sigma_{d6}/ C_{31}^{uB} ^2$	0.469	0.485	0.451	0.376
$WW$	0.263	0.371	0.454	0.486
$Wjj$	0.00773	0.0190	0.0184	0.0205
$Zjj$	0.302	0.425	0.554	0.516
$tb$	0.122	0.282	0.471	0.485
SM	0.694	1.065	1.497	1.508

Table 9: Cross sections in fb for the signal process (14) with  $C_{13,31}^{uW,uB} = 1$  one at a time, and all other effective FC couplings vanishing, and for SM background processes: doubly-resonant  $W$  production (labeled  $WW$ ), singly-resonant  $W$  ( $Wjj$ ) and  $Z$  ( $Zjj$ ) productions, and single-top production ( $tb$ ). The sum of all backgrounds is labeled SM. All cross sections computed with the cuts (16)–(19).

We obtain limits on the effective FC couplings  $|C_{13,31}^{uW}|$  and  $|C_{13,31}^{uB}|$  from the relation,

$$N_{d6} < \mathcal{S} \Delta_{\text{tot}} N_{\text{SM}}, \quad (20)$$

where  $\mathcal{S}$  is the statistical significance, and

$$N_{d6} = \sigma_{d6} L_{\text{int}} = |C_{13,31}^{uW,uB}|^2 \left( \frac{\sigma_{d6}}{|C_{13,31}^{uW,uB}|^2} \right) L_{\text{int}}, \quad N_{\text{SM}} = \sigma_{\text{SM}} L_{\text{int}}, \quad (21)$$

$$\Delta_{\text{tot}} N_{\text{SM}} = \sqrt{(\Delta_{\text{stat}} N_{\text{SM}})^2 + (\Delta_{\text{syst}} N_{\text{SM}})^2}, \quad \Delta_{\text{stat}} N_{\text{SM}} = \sqrt{\sigma_{\text{SM}} L_{\text{int}}}, \quad \Delta_{\text{syst}} N_{\text{SM}} = \varepsilon_{\text{syst}} \sigma_{\text{SM}} L_{\text{int}},$$

$\sqrt{s}$ [TeV]	3	6	10	14		$\sqrt{s}$ [TeV]	3	6	10	14
	$\varepsilon_{\text{syst}} = 0.00$									
$ C_{13}^{uW}  <$	0.145	0.0797	0.0574	0.0442		$ C_{13}^{uB}  <$	0.251	0.199	0.183	0.168
$ C_{31}^{uW}  <$	0.138	0.0276	0.0511	0.0390		$ C_{31}^{uB}  <$	0.237	0.183	0.165	0.152
	$\varepsilon_{\text{syst}} = 0.02$									
$ C_{13}^{uW}  <$	0.154	0.102	0.0934	0.0840		$ C_{13}^{uB}  <$	0.267	0.255	0.298	0.319
$ C_{31}^{uW}  <$	0.147	0.0931	0.0831	0.0741		$ C_{31}^{uB}  <$	0.252	0.235	0.268	0.289

Table 10: Single-coupling limits on  $|C_{13,31}^{uW,uB}|$  at statistical significance  $\mathcal{S} = 1$  (68% C.L.) from (20) for systematic uncertainty  $\varepsilon_{\text{syst}} = 2\%$ . Limits for  $\varepsilon_{\text{syst}} = 0\%$  are also shown for comparison.

with  $(\sigma_{d6}/|C_{13,31}^{uW,uB}|^2)$  taken from the first two lines of table 9,  $\sigma_{\text{SM}}$  from the last line of that table, and the integrated luminosity  $L_{\text{int}}$  from table 1. The relative systematic uncertainty  $\varepsilon_{\text{syst}}$ , which must be experimentally established, is tentatively set in this paper to 2%,  $\varepsilon_{\text{syst}} = 0.02$ . The limits on  $|C_{k3,3k}^{uW,uB}|$ ,  $k = 1, 2$ , obtained from (20) are shown in table 10 for four values of  $\sqrt{s}$ . As expected, in view of the increasing cross sections in table 9, the sensitivity is higher the larger the collision energy. Also shown in the table are limits obtained for purely statistical uncertainty,  $\varepsilon_{\text{syst}} = 0$ , to assess the relative importance of statistical and systematic uncertainties.

## 5 Conclusions

Based on the processes of FC single top-quark production at a high energy MuC, we have estimated individual limits on dimension-six operators of the SMEFT basis [23]. In particular, we have identified a comprehensive list of nine operators that generate top quark-gauge boson couplings and seven four-fermion operators for the contact terms  $\mu\bar{\mu}tu$ . Based on the potential yields on the cross sections and the current limits in the literature we have found that the MuC can have widely different sensitivities to these operators. Operators  $Q_{\varphi ud}$  and  $Q_{dW}$  get very weak constraints of  $O(10^1)$ , whereas  $Q_{uW}$  and  $Q_{uB}$  get limits of  $O(10^{-2})$ . Four-fermion operators get limits of  $O(10^{-4})$  while current limits are of order 1. Below we present a detailed list of the specific conclusions of our study.

- (1) There are seven four-fermion operators in the Warsaw basis that contribute to  $t\bar{u}$  (and  $u\bar{t}$ ) production. We define two combinations that separate  $\mu\bar{\mu}tu$  and  $\mu\bar{\mu}bd$  contact terms so we reduce the list to six operators. Since the cross sections grow with  $s$ , the limits we obtain are three to four orders of magnitude smaller than the current limits from LEP and LHC data.
- (2) Concerning fermion-boson operators, two of them stand out as the most relevant for FC top production at the MuC:  $Q_{uB}$  and  $Q_{uW}$ . At tree level they are not sensitive to  $B$  measurements nor FC bottom quark production. For energies 6 – 14 TeV the MuC would give better limits to these two operators than the current 2023 LHC bounds (see table 3), though the future HL-LHC might yield similar limits. The two most important processes are  $\mu^+\mu^- \rightarrow t\bar{q}$  and  $\mu^+\mu^- \rightarrow t\bar{q}\nu\bar{\nu}$ , with  $\nu$  representing the contribution from the three neutrino flavors. The limits from these two processes are given in tables 4 and 7, respectively (see also table 5, for limits from radiative top production).
- (3)  $C_{k3}^{uB}$  and  $C_{3k}^{uB}$  get better limits from the two-to-two process  $\mu^+\mu^- \rightarrow t\bar{q} + \bar{t}\bar{q}$  than from  $\mu^+\mu^- \rightarrow t\bar{q}\nu\bar{\nu} + \bar{t}\bar{q}\nu\bar{\nu}$ , see table 4. For the latter process with  $\nu = \nu_\mu$ , a strong destructive interference occurs between the  $WW$  fusion diagrams with  $\gamma$  and  $Z$  propagators. Therefore,  $WW$  fusion only gives a very small contribution and we have found that for this operator in particular the EWA does not apply. This would not be an isolated case where the approximation differs from the full calculation. Some years ago a study on the validity of the EWA for (SM)  $e^+e^- \rightarrow W^+W^-\nu_e\bar{\nu}_e$  at  $\sqrt{s} = 2\text{TeV}$  found substantial deviations in some kinematical regions [51].

- (4) For the case of  $\mu^+\mu^- \rightarrow t\bar{q}\nu\bar{\nu}$ ,  $C_{k3}^{uW}$  and  $C_{3k}^{uW}$  ( $k = 1, 2$ ) are the coefficients that get the strongest limits. For a MuC at 10 TeV and  $10\text{ab}^{-1}$  integrated luminosity they can be one third lower than the current limits from  $t \rightarrow u\gamma$  at the LHC. See table 10 for limits from the hadronic decay channel of associate top production  $\mu^+\mu^- \rightarrow t\bar{q}\nu\bar{\nu}$ .
- (5)  $C_{k+3}^{\varphi u}$  gets competitive limits only from the  $WW$  fusion diagram in  $\mu^+\mu^- \rightarrow t\bar{q}\nu_\mu\bar{\nu}_\mu$  and not from  $\mu^+\mu^- \rightarrow t\bar{q}$ . See table 8 in section 3.4. Notice, moreover, that unlike the other operators in that table,  $Q_{\varphi u}^{k+3}$  does not contribute to  $B$  decays at tree level.
- (6) Concerning  $Q_{\varphi q(-)}$ , the MuC would only provide limits that are already twice as large as the current LHC limits that come from  $t \rightarrow uZ$  decay. In addition to this,  $Q_{\varphi q(-)}$  also generates a left handed  $Wub$  coupling that is sensitive to  $B$  meson measurements at tree level. (See table 8 for our constraints on this coupling from  $\mu^+\mu^- \rightarrow t\bar{q}\nu\bar{\nu}$  production.)
- (7) Clearly, operators that generate FCNC  $Zbd$  and  $\gamma bd$  couplings should be probed by single bottom quark production rather than top production. However, we point out that  $C_{k+3}^{\varphi q(+)}$  in particular might also be probed successfully even with  $t\bar{q}\nu_\mu\bar{\nu}_\mu$  production (see table 8).
- (8) As observed in section 3.3,  $C_{k3(3k)}^{uG}$  could be probed with the  $t\bar{u}g$  production, but the sensitivity is expected to be about one order of magnitude weaker than current LHC limits. Thus,  $Q_{uG}^{k3(3k)}$  is the third low-sensitivity operator. We remark, however, that this operator plays an important role in global analyses at NLO in QCD [25].
- (9) As discussed in section 3.4, the sensitivity of the MuC top-production processes to  $Q_{dW}$  and  $Q_{\varphi ud}$  is very low, as a result of the their very small cross sections. Their contribution to  $t\bar{q}\nu_\mu\bar{\nu}_\mu$  production is either zero for  $C_{3k}^{\varphi ud}$  and  $C_{3k}^{dW}$ , or nevertheless negligible for  $C_{k3}^{\varphi ud}$  and  $C_{k3}^{dW}$  (see eq. (13)). Taking into account also that both operators get stringent constraints from  $B$  measurements, we conclude that they can be safely discarded from future studies outright.
- (10) Finally, we remark that some operator coefficients are associated with couplings that do not involve the top quark. In particular,  $C_{1+3}^{\varphi q(-)}$ ,  $C_{1+3}^{\varphi q(+)}$ ,  $C_{13}^{\varphi ud}$  and  $C_{31}^{uW}$  generate a  $Wub$  vertex, and  $C_{31}^{dW}$  and  $C_{13}^{dW}$  generate a  $Zbd$  vertex. All these operators get strong constraints from  $B$  meson measurements.

**Acknowledgments** We are grateful to Georgina Espinoza Gurriz for her assistance with our computer hardware. We acknowledge support from Sistema Nacional de Investigadores de Conacyt, México. We acknowledge that an arXiv has previously been published [52].

## References

- [1] C. Accettura, D. Adams, R. Agarwal, *et al.*, “Towards a muon collider,” Eur. Phys. J. C **83**, no.9, 864 (2023), [erratum: Eur. Phys. J. C **84**, no.1, 36 (2024)].
- [2] K. M. Black, S. Jindariani, D. Li, F. Maltoni, *et al.* “Muon Collider Forum Report,” JINST **19**, no.02, T02015 (2024).
- [3] H. Al Ali, N. Arkani-Hamed, I. Banta, *et al.* “The muon Smasher’s guide,” Rept. Prog. Phys. **85**, no.8, 084201 (2022).
- [4] R. Franceschini and M. Greco, “Higgs and BSM Physics at the Future Muon Collider,” Symmetry **13** (2021) no.5, 851.
- [5] M. Chiesa, F. Maltoni, L. Mantani, B. Mele, F. Piccinini and X. Zhao, “Measuring the quartic Higgs self-coupling at a multi-TeV muon collider,” JHEP **09**, 098 (2020).

- [6] M. Forslund and P. Meade, “High precision higgs from high energy muon colliders,” JHEP **08**, 185 (2022).
- [7] M. Forslund and P. Meade, “Precision Higgs width and couplings with a high energy muon collider,” JHEP **01**, 182 (2024).
- [8] B. Abbott, A. Apyan, B. Azartash-Namin, V. Balakrishnan, J. Berryhill, S. C. Hsu, S. Jindariani, M. P. Kawale, E. E. Khoda and R. Parsons, A. Schuy, M. Strauss, J. Stupak and C. Waits, “Anomalous production of massive gauge boson pairs at muon colliders,” Phys. Rev. D **108**, no.9, 093009 (2023).
- [9] J. C. Yang, Z. B. Qing, X. Y. Han, Y. C. Guo and T. Li, “Tri-photon at muon collider: a new process to probe the anomalous quartic gauge couplings,” JHEP **22**, 053 (2020).
- [10] J. Chen, T. Li, C. T. Lu, Y. Wu and C. Y. Yao, “Measurement of Higgs boson self-couplings through  $2 \rightarrow 3$  vector bosons scattering in future muon colliders,” Phys. Rev. D **105**, no.5, 053009 (2022).
- [11] Z. Liu, K. F. Lyu, I. Mahbub and L. T. Wang, “Top Yukawa coupling determination at high energy muon collider,” Phys. Rev. D **109**, no.3, 035021 (2024).
- [12] A. Belyaev, R. S. Chivukula, B. Fuks, E. H. Simmons and X. Wang, “Vectorlike top quark production via an electroweak dipole moment at a muon collider,” Phys. Rev. D **108**, no.3, 3 (2023).
- [13] A. Azatov, F. Garosi, A. Greljo, D. Marzocca, J. Salko and S. Trifinopoulos, “New physics in  $b \rightarrow s\mu\mu$ : FCC-hh or a muon collider?,” JHEP **10**, 149 (2022).
- [14] A. Greljo, J. Salko, A. Smolkovič and P. Stangl, “SMEFT Restrictions On Exclusive  $b \rightarrow u\ell\nu$  Decays,” JHEP **11**, 023 (2023).
- [15] W. Altmannshofer, S. A. Gadam and S. Profumo, “Probing New Physics with  $\mu^+\mu^- \rightarrow bs$  at a Muon Collider,” Phys. Rev. D **108**, no.11, 115033 (2023).
- [16] J. C. Yang, X. Y. Han, Z. B. Qin, T. Li and Y. C. Guo, “Measuring the anomalous quartic gauge couplings in the  $W^+W^- \rightarrow W^+W^-$  process at muon collider using artificial neural networks,” JHEP **09**, 074 (2022).
- [17] P. Asadi, R. Capdevilla, C. Cesariotti and S. Homiller, “Searching for leptoquarks at future muon colliders,” JHEP **10**, 182 (2021).
- [18] S. Homiller, Q. Lu and M. Reece, “Complementary signals of lepton flavor violation at a high-energy muon collider,” JHEP **07**, 036 (2022).
- [19] K. Fridell, R. Kitano and R. Takai, “Lepton flavor physics at  $\mu^+\mu^-$  colliders,” JHEP **06**, 086 (2023).
- [20] T. Li, C. Y. Yao and M. Yuan, “Searching for heavy neutral lepton and lepton number violation through VBS at high-energy muon colliders,” JHEP **09**, 131 (2023).
- [21] W. Yin and M. Yamaguchi, “Muon  $g-2$  at a multi-TeV muon collider,” Phys. Rev. D **106** (2022) 033007.
- [22] F. Larios, R. Martinez and M. A. Perez, “New physics effects in the flavor-changing neutral couplings of the top quark,” Int. J. Mod. Phys. A **21**, 3473-3494 (2006).

- [23] B. Grzadkowski, M. Iskrzynski, M. Misiak and J. Rosiek, “Dimension-Six Terms in the Standard Model Lagrangian,” *JHEP* **10**, 085 (2010).
- [24] A. Dedes, W. Materkowska, M. Paraskevas, J. Rosiek and K. Suxho, “Feynman rules for the Standard Model Effective Field Theory in  $R_\epsilon$ -gauges,” *JHEP* **06**, 143 (2017).
- [25] G. Durieux, F. Maltoni and C. Zhang, “Global approach to top-quark flavor-changing interactions,” *Phys. Rev. D* **91**, (2015) 074017.
- [26] G. Isidori, F. Wilsch and D. Wyler, “The standard model effective field theory at work,” *Rev. Mod. Phys.* **96**, no.1, 015006 (2024).
- [27] A. O. Bouzas and F. Larios, “Two-to-Two Processes at an Electron-Muon Collider,” *Adv. High Energy Phys.* **2022**, 3603613 (2022).
- [28] A. Escamilla, A. O. Bouzas and F. Larios, “Single top production at linear  $e^-e^+$  colliders,” *Phys. Rev. D* **97**, 033004 (2018).
- [29] L. Shi and C. Zhang, “Probing the top quark flavor-changing couplings at CEPC,” *Chin. Phys. C* **43**, no.11, 113104 (2019).
- [30] W. Altmannshofer, S. Gori, B. V. Lehmann and J. Zuo, “UV physics from IR features: New prospects from top flavor violation,” *Phys. Rev. D* **107**, no.9, 095025 (2023).
- [31] H. Khanpour, S. Khatibi, M. Khatiri Yanehsari and M. Mohammadi Najafabadi, “Single top quark production as a probe of anomalous  $tq\gamma$  and  $tqZ$  couplings at the FCC-ee,” *Phys. Lett. B* **775**, 25-31 (2017).
- [32] S. Khatibi and M. Moallemi, “Probing FCNC couplings in single top-quark production associated with a neutral gauge boson in future lepton colliders,” *J. Phys. G* **48**, no.12, 125004 (2021).
- [33] Y. Afik, S. Bar-Shalom, A. Soni and J. Wudka, “New flavor physics in di- and trilepton events from single-top production at the LHC and beyond,” *Phys. Rev. D* **103**, no.7, 075031 (2021).
- [34] S. Sun, Q. S. Yan, X. Zhao and Z. Zhao, “Constraining rare B decays by  $\mu^+\mu^- \rightarrow t\bar{c}$  at future lepton colliders,” *Phys. Rev. D* **108**, no.7, 7 (2023).
- [35] L. Cremer, J. Erdmann, R. Harnik, J. L. Späh and E. Stamou, “Leveraging on-shell interference to search for FCNCs of the top quark and the Z boson,” *Eur. Phys. J. C* **83**, no.9, 871 (2023).
- [36] C. H. Chen and T. Nomura, “Scotogenic top-quark FCNC decays,” *Phys. Rev. D* **106**, no.9, 095005 (2022).
- [37] W. George, “Searches for rare top quark production and decay processes with the ATLAS experiment,” [arXiv:2307.04664 [hep-ex]].
- [38] J. Alwall, R. Frederix, S. Frixione, V. Hirschi, F. Maltoni, O. Mattelaer, H. S. Shao, T. Stelzer, P. Torrielli and M. Zaro, “The automated computation of tree-level and next-to-leading order differential cross sections, and their matching to parton shower simulations,” *JHEP* **07**, 079 (2014).
- [39] A. Alloul, N. D. Christensen, C. Degrande, C. Duhr and B. Fuks, *Comput. Phys. Commun.* **185**, 2250-2300 (2014).
- [40] R. Brun, F. Rademakers, “ROOT — An object oriented data analysis framework,” *Nucl. Instrum. Methods Phys. Res. A* **389** (1997) 81.

- [41] A. Belyaev, N. D. Christensen and A. Pukhov, “CalcHEP 3.4 for collider physics within and beyond the Standard Model,” *Comput. Phys. Commun.* **184**, 1729-1769 (2013).
- [42] S. L. Glashow, J. Iliopoulos and L. Maiani, “Weak Interactions with Lepton-Hadron Symmetry,” *Phys. Rev. D* **2**, 1285-1292 (1970).
- [43] W. Altmannshofer, “TASI 2022 lectures on flavor physics,” PoS **TASI2022**, 001 (2024).
- [44] R. Ruiz, A. Costantini, F. Maltoni and O. Mattelaer, “The Effective Vector Boson Approximation in high-energy muon collisions,” *JHEP* **06**, 114 (2022).
- [45] T. Corbett, O. J. P. Éboli and M. C. Gonzalez-Garcia, “Unitarity Constraints on Dimension-six Operators II: Including Fermionic Operators,” *Phys. Rev. D* **96**, no.3, 035006 (2017).
- [46] G. Isidori, Y. Nir and G. Perez, “Flavor Physics Constraints for Physics Beyond the Standard Model,” *Ann. Rev. Nucl. Part. Sci.* **60**, 355 (2010).
- [47] G. Aad *et al.* [ATLAS], “Search for flavor-changing neutral  $tqH$  interactions with  $H \rightarrow \gamma\gamma$  in  $pp$  collisions at  $\sqrt{s} = 13$  TeV using the ATLAS detector,” *JHEP* **12**, 195 (2023).
- [48] M. E. Cassidy, Z. Dong, K. Kong, I. M. Lewis, Y. Zhang, Y. J. Zheng, “Probing the CP Structure of the Top Quark Yukawa at the Future Muon Collider,” [arXiv:2311.07645 [hep-ph]].
- [49] A. Crivellin, M. Kirk, T. Kitahara, F. Mescia, “Large  $t \rightarrow cZ$  as a sign of vectorlike quarks in light of the W mass,” *Phys. Rev. D* **106** (2022) L031704.
- [50] R. L. Workman *et al.* (Particle Data Group), “Review of Particle Physics,” *Prog. Theor. Exp. Phys.* 2022, 083C01 (2022) and 2023 update.
- [51] W. Bernreuther and L. Chen, “Improved effective vector boson approximation revisited,” *Phys. Rev. D* **93**, no.5, 053018 (2016).
- [52] D. Ake, A. O. Bouzas and F. Larios, “Top quark flavor changing couplings at a muon collider,” [arXiv:2311.09488 [hep-ph]].

## A From gauge to mass eigenstates.

In this work we follow the same definitions of Wilson coefficients and the Feynman rules as given in ref. [24] for all operators except for the operators  $Q_{\varphi q}^{(1)}$  and  $Q_{\varphi q}^{(3)}$ . In [24] they use  $U_{d_L}$  to redefine the Wilson coefficients  $C'^{\varphi q(1)}$  and  $C'^{\varphi q(3)}$ . In our case we use  $U_{u_L}$  for  $C'^{\varphi q(-)}$ , and  $U_{d_L}$  for  $C'^{\varphi q(+)}$ :

$$C^{\varphi q(-)} = U_{u_L}^\dagger C'^{\varphi q(-)} U_{u_L}, \quad C^{\varphi q(+)} = U_{d_L}^\dagger C'^{\varphi q(+)} U_{d_L}.$$

Comparing with the Feynman rule for the  $Ztu$  coupling in [24] we have

$$C_{13(31)}^{\varphi q(-)} \simeq V_{ud} V_{tb} (\mathbf{C}_{13(31)}^{\varphi q1} - \mathbf{C}_{13(31)}^{\varphi q3}), \quad (22)$$

where  $\mathbf{C}_{13(31)}^{\varphi q(1,3)}$  are the Wilson coefficients in [24] and we have omitted terms proportional to non-diagonal CKM elements. As mentioned above, operators  $Q_{\varphi u}$  and  $Q_{\varphi q}^{(\pm)}$  are Hermitian. Therefore, when we rotate to mass eigenstates the coefficients in  $C^{\varphi u}$  and  $C^{\varphi q(\pm)}$  are taken as Hermitian  $3 \times 3$  matrices. Then, the matrix elements can be written as (see [25]):

$$C_{a3}^{\varphi q(\pm)} = C_{3a}^{\varphi q(\pm)*} \equiv C_{a+3}^{\varphi q(\pm)}, \quad C_{a3}^{\varphi u} = C_{3a}^{\varphi u*} \equiv C_{a+3}^{\varphi u},$$

for  $a = 1, 2$ . The effective Lagrangian is then written as a sum of operators in mass eigenstate basis along with their coefficients, with the non-Hermitian operators added their Hermitian conjugate term.

## B LHC bounds on effective top couplings

The following limits are obtained from FCNC  $Br(t \rightarrow Vq)$ ,  $V = g, \gamma, Z, H$  recent bounds from the LHC [37]

$$\begin{aligned}
(t \rightarrow u\gamma) \quad & |C_{13(31)}^{uB}| \leq 0.037, \quad |C_{13(31)}^{uW}| \leq 0.066 \\
(t \rightarrow uZ) \quad & |C_{13(31)}^{uB}| \leq 0.23, \quad |C_{13(31)}^{uW}| \leq 0.13 \\
(t \rightarrow uZ) \quad & |C_{1+3}^{\varphi u}| \leq 0.19, \quad |C_{1+3}^{\varphi q(-)}| \leq 0.10 \\
(t \rightarrow uH) \quad & |C_{13(31)}^{u\varphi}| \leq 1.2, \quad (t \rightarrow ug)|C_{13(31)}^{uG}| \leq 0.074 \\
(t \rightarrow c\gamma) \quad & |C_{23(32)}^{uB}| \leq 0.081, \quad |C_{23(32)}^{uW}| \leq 0.15 \\
(t \rightarrow cZ) \quad & |C_{23(32)}^{uB}| \leq 0.34, \quad |C_{23(32)}^{uW}| \leq 0.19 \\
(t \rightarrow cZ) \quad & |C_{2+3}^{\varphi u}| \leq 0.28, \quad |C_{2+3}^{\varphi q(-)}| \leq 0.14 \\
(t \rightarrow cH) \quad & |C_{23(32)}^{u\varphi}| \leq 1.4, \quad (t \rightarrow cg)|C_{23(32)}^{uG}| \leq 0.18
\end{aligned} \tag{23}$$